Saudi Pharmaceutical Journal 26 (2018) 1162–1169

Contents lists available at ScienceDirect

Saudi Pharmaceutical Journal

journal homepage: www.sciencedirect.com

Original article

Targeting of somatostatin receptors expressed in blood cells using quantum dots coated with vapreotide

Ahmed A.H. Abdellatif [a,b,*], Heba A. Abou-Taleb [c], Ahmed A. Abd El Ghany [d], Ilka Lutz [e], Abdellatif Bouazzaoui [f,g]

[a] Pharmaceutics and Industrial Pharmacy Department, Faculty of Pharmacy, Al-Azhar University, 71524 Assiut, Egypt
[b] Pharmaceutics Department, Faculty of Pharmacy, Qassim University, 51452 Buraydah, Saudi Arabia
[c] Pharmaceutics and Industrial Pharmacy Department, Faculty of Pharmacy, Nahda University (NUB), Benisuef, Egypt
[d] Biochemistry Department, Faculty of Pharmacy, Al-Azhar University, Assiut, Egypt
[e] Leibniz-Institute of Freshwater Ecology and Inland Fisheries, Mueggelseedamm 301, 12587 Berlin, Germany
[f] Science and Technology Unit, Umm Al Qura University, Makkah 21955, Saudi Arabia
[g] Internal Medicine 3-Hematology/Oncology Department, University Medical Center, Regensburg, Germany

ARTICLE INFO

Article history:
Received 17 March 2018
Accepted 19 July 2018
Available online 20 July 2018

Keywords:
Quantum dots
Vapreotide
Somatostatin
Blood
Receptor
Targeting

ABSTRACT

Cancer may be difficult to target, however, if cancer targeted this provides the chance for a better and more effective treatment. **Q**uantum dots (Qdots) coated vapreotide (VAP) as a somatostatin receptors (SSTRs) agonist can be efficient targeting issue since may reduce side effects and increase drug delivery to the target tissue. This study highlights the active targeting of cancer cells by cells imaging with improving the therapeutic outcomes. VAP was conjugated to Qdots using amine-to-sulfhydryl crosslinker. The synthesized Qdots-VAP was characterized by determination of size, measuring the zeta-potential and UV fluorometer. The cellular uptake was studied using different cell lines. Finally, the Qdots-VAP was injected into a rat model. The results showed a size of 479.8 ± 15 and 604.88 ± 17 nm for unmodified Qdots and Qdots-VAP respectively, while the zeta potential of particles went from negative to positive charge which proved the conjugation of VAP to Qdots. The fluorometer recorded a redshift for Qdots-VAP compared with unmodified Qdots. Moreover, cellular uptake exhibited high specific binding with cells which express SSTRs using confocal microscopy and flow cytometry (17.3 MFU comparing to 3.1 MFU of control, $P < 0.001$). Finally, an *in vivo* study showed a strong accumulation of Qdots-VAP in the blood cells (70%). In conclusion, Qdots-VAP can play a crucial role in cancer diagnosis and treatment of blood cells diseases when conjugated with VAP as SSTRs agonist.

1. Introduction

It is problematic to distinguish and to specifically treat the cancer cells, nevertheless, if cancer expresses a specific receptor such as somatostatin receptors (SSTRs) will offer the chance for more effective and specific targeting. Targeting techniques have become of crucial importance for the early detection by imaging of various types of cancers today, imaging is simply a method for the detection and to determine the stages and the exact locations of cancer. In order to check whether it has returned all of which can assist in directing surgery and cancer therapy (Akita et al., 2016, Potier et al., 2016). Clinical trials play a significant role in order to prove whether the imaging techniques are more efficient and safe than radiological procedures and therapies. These methods include images from diagnostic radiology, interventional radiology, and radiation therapy (Derwin et al., 2012). These types of radiations have many side effects as it can also induce cancer (Pilz et al., 2016; Schneider et al., 2016). Some other additional kinds of imaging techniques are safe and easy to use (Li et al., 2013). Moreover, the targeted transference of NPs to site-specific cells could be distributed to a specific organ in the body and therefore reduce side effects and toxic reactions significantly (Bertrand and Leroux, 2012; Othman et al., 2017). This kind of treatment will

* Corresponding author at: Faculty of Pharmacy, Qassim University, Saudi Arabia.
E-mail addresses: a.abdellatif@qu.edu.sa, ahmed.a.h.abdellatif@azhar.edu.eg (A.A.H. Abdellatif).
Peer review under responsibility of King Saud University.

Production and hosting by Elsevier

https://doi.org/10.1016/j.jsps.2018.07.004
1319-0164/

deliver the drug specifically to only the cancer cells, and hence will be safe for the other healthy cells. Our strategy is safely targeting the cancer cells through receptor as a kind of active targeting. The active targeting, also named ligand-mediated targeting, includes attaching ligands to the surface of nanoparticles (NPs) for specific uptake by the targeted diseased cells. Ligands are usually chosen to bind surface molecules or receptors that are over-expressed in diseased cells, tissues or subcellular areas (Avvakumova et al., 2016; Kwon et al., 2016). Active targeting is aimed towards enhancing interactions between NPs and receptors as well as increasing internalization of NPs without changing the overall NPs bio-distribution (Abdellatif et al., 2016). Active targeting may also avoid the non-specific binding of proteins during the NP's journey through the bloodstream which affects the targeting efficiency of NPs. This may be improved by altering the physiochemical properties such as the ligand density, the size of the formulated or the choice of the attached targeting ligand *in vitro* as well as *in vivo* (Phatak et al., 2007; Cheng et al., 2013). The formulated NPs can be identified using different methods that are a novel approach for cancer-targeting.

The receptor selected for this targeting is SSTRs, which are parts of the G protein-coupled receptors (GPCRs) (Hoyer et al., 1995; Patel, 1999). There are five subtypes of SSTRs (SSTR1-5) which are expressed in many organs such as the pancreas, kidney, heart blood cells and cancer cells. SSTRs can be targeted using somatostatin (SST) or its analogues such as octreotide (OCT) and vapreotide (VAP). The SSTRs are either expressed on the cell membrane or within the cell, and cells that do not have such receptors cannot be influenced directly by that SST or SST analogues (Abdellatif et al., 2016). Significantly, it was reported that SSTRs are over-expressed in all kinds of cancer. Additionally, it was proven in our lab that cancer cells express SSTRs, and therefore delivering drug to cancer is possible by targeting SSTR2, and imaging also is possible by using NPs with high fluorescence, such as Quantum dots (Qdots) (Herrmann et al., 2015; Gupta et al., 2017).

Qdots are a semiconductor, having huge advantages for *in vivo* applications because they resist photobleaching (Chen et al., 2009) and provides a good stability in the bloodstream (Ballou et al., 2005). In addition, amine-PEGylated Qdots have low cytotoxicity when incubated with cell culture, which makes Qdots suitable tools for cellular and molecular imaging techniques, used to diagnose the nature and stage of cancer and other diseases. Consequently, Qdots conjugated VAP can be used to transport a certain number of drugs to specific sites in the human body. Qdots have distinctive chemical and physical possessions due to their characteristic size and their high compacted structure (Ghasemi et al., 2009).

The aim of this study is to develop and formulate novel Qdots conjugated with SST analogues which is VAP for targeting $SSTR_2$ expressed in blood cells. The selected Qdots which have both fluorescences and can deliver the drug to a specific site. For this, Qdots coated with VAP (Qdots-VAP) were formulated. For selective binding to $SSTR_2$, the Qdots-VAP was incubated using MCF7 cells which expressed all kind of SSTRs. Flow cytometry (FACs) and confocal laser scanning microscopy (CLSM) were used for imaging the fluorescent of Qdots-VAP in the MCF7. Finally, the formulated Qdots-VAP were injected into model rats. Thus, this state of art groundbreaking methodology will open new approaches for the specific targeting of cancer cells.

2. Materials and methods

2.1. Materials

Quantum dots carrying PEG-amine, Dulbecco's phosphate buffered saline (pH 7.2), Dulbecco's Modified Eagle Medium, and Leibovitz's L-15 and Sulfo-SMCC (sulfosuccinimidyl 4-(N-maleimidomethyl)-cyclohexane-1-carboxylate) from Life Technologies Ltd, Paisley PA4 9RF, U.K. Triethanolamine buffer and Ethylene di-amin Tetraacetic acid (EDTA) were purchased from Sigma Aldrich (Steinheim, Germany). Human Caucasian breast adenocarcinoma (MCF7 cells) were purchased from VACSERA CO., Dukki, Giza, Egypt. Adult female albino rats (each 120-130 g) with age of about 6–8 months were used for the *in-vivo* experiment. The rats were housed under harmonized environmental situations in the pre-clinical animal house, Department of Pharmacology, Faculty of Medicine, Assiut University, Assiut. They were fed with typical diet and permitted free access to drinking water.

2.2. Conjugation of vapreotide to quantum dots

In order to conjugate VAP to Qdots-PEG-amine, VAP was first thiolated using Traut's reagent. For thiolation of VAP, it was dissolved in phosphate buffer (pH 8.2, 0.1 M). Typically, 500 μL of 1.2 mM VAP was mixed with an equimolar concentration of Traut́s reagent. The reactants were incubated at 37 °C and stirred at 600 rpm for 60 min (Amartey, 1993). The reaction mixture was purified using Sephadex G-25 mini-column (Updegrove et al., 2011). Furthermore, Qdots-PEG-amine was activated with a 500-fold molar excess of sulfo-SMCC. The activated Qdots-sulfo-SMCC was conjugated to the thiolated-VAP to form Qdots-VAP. The reactants were incubated at 37 °C and stirred at 600 rpm for 3 h at pH 7. The final product was purified by centrifugation using an ultrafiltration tube (Amicon Ultra-4, 100 K MWCO; GE Healthcare) (Fig. 1).

2.3. Characterization of nanoparticles

2.3.1. Dynamic light scattering

The dynamic light scattering (DLS) was used to determine the size, count rate and zeta potential of Qdots-PEG-amine (before and after conjugation with VAP). The samples were adjusted to 25 °C, then subjected to a laser beam of 633 nm at a scattering angle of 90° using the Malvern Zetasizer nano s90 (Malvern Instruments GmbH, Herrenberg, Germany) (Leung et al., 2006, Destremaut et al., 2009). All samples were placed in aqueous solution. The results were calculated from the average of the three measurements while each measurement was run 20 times (10 s duration).

2.3.2. Spectrophotometric analysis

The fluorescence of Qdots-PEG-amine (before and after conjugation with VAP) was recorded using a Perkin-Elmer LS 55 (Perkin Elmer, Waltham, U.S.A.) equipped with a R928 red-sensitive quantum photomultiplier and the FL-WinLab V4.00.03 software in 1 cm quartz cuvettes and in polycarbonate crystal microplates in white to provide maximum reflectivity, and for allowing high sensitivity of the luminescence/fluorescence assays. The fluorescence emission spectra of VAP in phosphate buffer pH 7.2 were recorded. Excitation wavelength maximum of VAP was 288 nm and an emission wavelength maximum 305 nm. Fluorescence emission spectra were also recorded in order to determine the shift obtained after conjugation VAP to Qdots-PEG-amine using (Ex: 488 nm and Em: 655 nm) (Sreenivasan et al., 2012).

2.3.3. Cellular uptake

In order to study the cellular uptake and displacement of the formulated Qdots-VAP, (MCF7 cells passage 67) which express SSTRs as reported previously (Abdellatif, 2015a,b). MCF7 were incubated with Qdots-PEG-amine (before and after conjugation with VAP) as the previously reported method (Fang et al., 2013; Tsoi et al., 2013). For the displacement experiment, Qdots-VAP were incubated with 100 μM free VAP for 1 h at 37 °C. After 1-h incubation all Qdots were removed from the incubation medium,

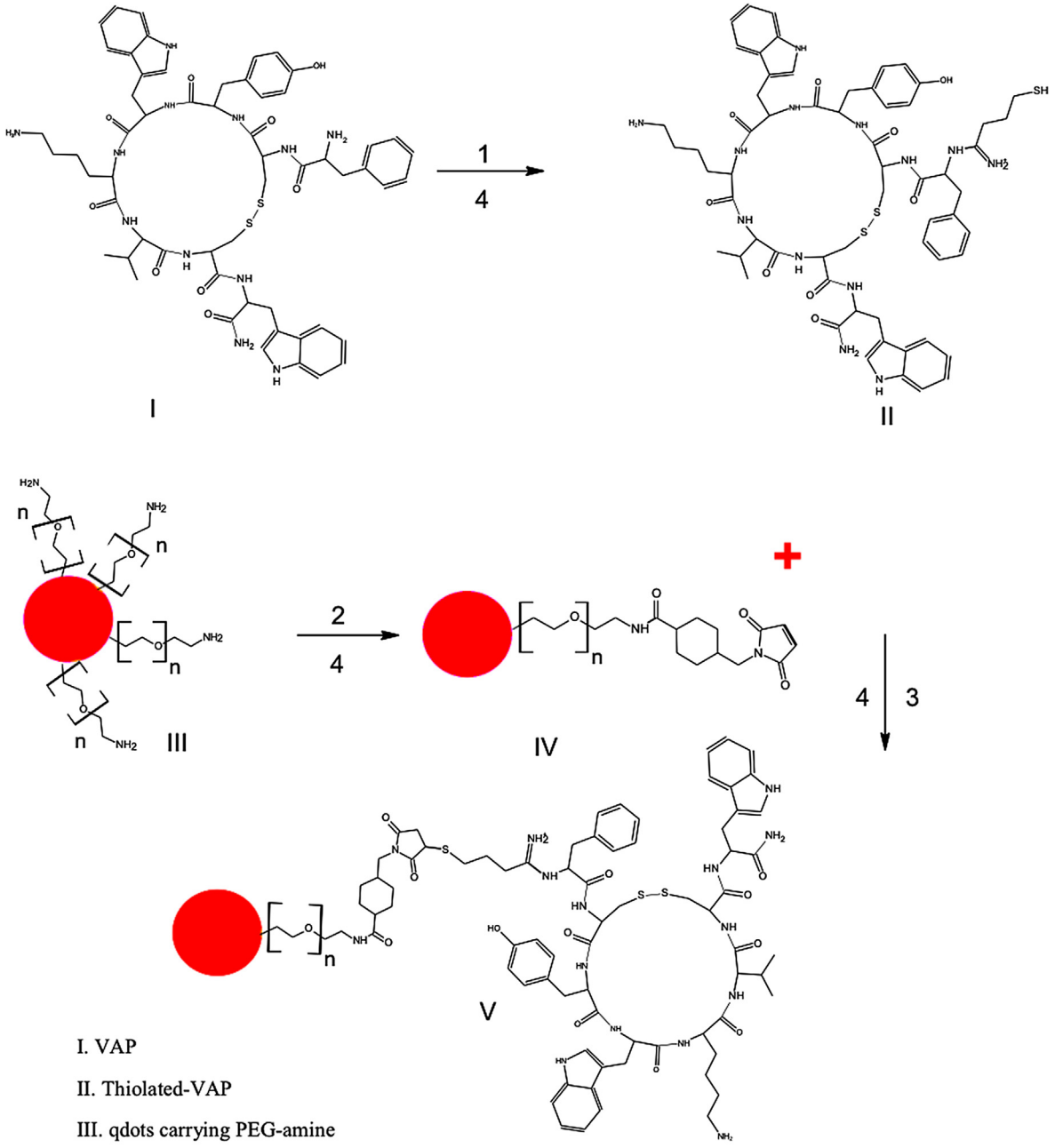

Fig. 1. Conjugation of Qdots-PEG-amine with VAP. Qdots was first activated using Sulfo-SMCC and then conjugated to VAP. The formulated Qdots-VAP was purified using Sephadex G-25.

the cells were washed with phosphate buffer pH 7.2 and afterward incubated with trypsin for 3 min. The cells were centrifuged at 1200 rpm at 4 °C, washed with phosphate buffer pH 7.2 and used for flow cytometry (FACS) analysis. Cells were analyzed on a FACS (Calibur BD Biosciences, San Jose, CA). Qdots were excited at 488 nm while the emission was measured using 655/16 nm band-pass filters. Data were calculated using Win-MDI 2.9 (The Scripps Institute, Flow Cytometry Core Facility), the software Windows Multiple Document Interface for Flow Cytometry. 10,000 cells were extracted and counted by FACS from the total amount of cells and the fluorescence was expressed in a histogram. Each record represents the average of three measurements (±SEM). The Qdots-PEG-amine concentration was determined prior to use fluorimetric measurement in a 96-well plate on an LS-55 fluorescence spectrometer at an excitation wavelength of 450 nm and an emission wavelength of 655 nm.

2.3.4. Identification of the internalized nanoparticles

For identification of the internalization of Qdots-VAP using confocal laser scanning microscopy (CLSM), 10,000 cells were seeded in an 8-well chamber-slide (Ibidi, Munich, Germany). To identify the specific interaction with receptors, a competitive displacement experiment was carried out by incubation of Qdots-VAP with a 1000-fold excess of free VAP as a competitor (Abdellatif and Tawfeek, 2016). The cells were incubated for 1 h at 37 °C, washed with DPBS and examined using a Zeiss Axiovert 200 M inverted epifluorescence microscope coupled with an LSM 510 laser scanning device, using a 40× plan-Apochromat water immersion objective (NA 1.2), CLSM (EX: 488/Em: 655).

2.3.5. Binding and displacement experiments

Binding and displacement experiments were carried out cell expressed receptors (Gupta et al., 1999), such as human breast cancer cell line MCF-7 cells expressing SSTR2. For the experiments, the cells were incubated with various concentrations of VAP with Qdots-VAP for 2 h at room temperature. Displacement trials were carried out using a fixed amount of 1 nM of Qdots-VAP while increasing the concentrations of the free VAP receptor agonist. Both, binding and displacement data were achieved after isolating the cells with trypsin. The fluorescence intensity was determined using a FACS Calibur (flow cytometer equipped with a 661/16 nm bandpass filter and an excitation laser of 488 nm).

2.3.6. In vivo study

In vivo studies were performed to examine the delivery of Qdots-VAP to blood cells. Adult female albino rats (n = 10) were used to prove the targeting of SSTRs. The rats were injected with 70 μL of ketamine (100 mg/kg) and xylazine (10 mg/kg) intraperitoneal at a ratio of (3:1). Afterward, the rats were injected with Qdots-PEG amine as a control and Qdots-VAP at a concentration of 100 pmol in the lateral vein (Abdellatif, 2015a,b). Animals were sacrificed after 1 h post-injection according to the previously described protocol (Davidson et al., 2015). Then the blood cells were collected and the peritoneal cavity was opened. The organs (liver, spleen, kidney, pancreas, lung, heart, tail, eyes) were dissected and fixed by immersion in 4% PFA for 24 h and eyes for 6 h. Inductively coupled plasma mass spectrometry (ICP-MS) was carried out to identify the amount of cadmium content of the Qdots-VAP in the organs and blood. All animal experiments were approved by the Research Ethics Committee in the Faculty of Medicine, Assiut University, Egypt.

2.3.7. Determination of cadmium mass using inductively coupled plasma-mass spectroscopy (ICP-MS)

The bio-distribution of Qdots-VAP was determined by measuring the cadmium mass in rat blood cells and the other organs using ICP-MS as recently described by Kane and Hall (2006), Wang et al. (2008). The amount of cadmium was quantified and then converted to the corresponding amount in kg using Microsoft excel program which makes the calculation easy. Briefly, the blood cells and all organ samples were digested by a microwave-assisted nitric acid digestion method using a MARSX press system (CEM). The cadmium content was determined, which corresponded (*) with the number of Qdots-VAP quantitatively. Concentrations of cadmium in the blood cells and organ samples were quantified using an ICP-MS 7700cx (Agilent Technologies, USA). The total injected dose (ID) per animal was calculated by adding up the cadmium mass of all organs.

2.3.8. Statistical analysis

All assays were carried out in triplicate. All data were expressed as a mean ± standard deviation. One-way analysis of variance and Bonferroni's post hoc test was used to analyze differences between the sets of data. A p-value smaller than 0.05 was considered significant.

3. Results

The unmodified Qdots-PEG-amine and the formulated Qdots-VAP were of a uniform particle size. The size was increased from 479.8 ± 15 to 604.88 ± 17 nm for Qdots-PEG-amine and Qdots-VAP respectively (Fig. 2). After purification, the Qdots-VAP was found to be stable without aggregation and the formulated Qdots-VAP were found also to be reasonably stable in size and didńt form aggregates. Qdots-PEG-amine displayed a zeta potential of −37.3 ± 6 mV. After conjugation with VAP, the zeta potential showed a reversal to positive values (+44 ± 3 mV) respectively (Fig. 3).

3.1. Fluorescence spectroscopy analysis

In order to explore the binding of VAP to Qdots-PEG-amine, the fluorescence spectra for VAP were measured in contrast to Qdots-VAP (Prescott et al., 2003). The results showed no considerable fluorescence emission when VAP was excited at 488 nm (Fig. 4). However, the significant redshift from 650 ± 3.6 to 661 ± 4.3 nm for Qdots-PEG-amine and Qdots-VAP respectively, $P < 0.001$ was observed when Qdots-PEG-amine and Qdots-VAP were excited at 488 nm at the same concentration (100 nM).

3.2. Cellular uptake

Qdots-VAP exhibited high specific binding to $SSTR_2$ when incubated with (MCF7 passage 67) but showed no significant uptake of unmodified Qdots-PEG-amine using confocal laser scanning microscopy (CLSM). In contrast, Qdots-VAP was internalized by the cells and showed as spots in the nucleus (Fig. 5). Qdots-VAP was found throughout the cells with strong fluorescence. Moreover, the experiments showed that the internalization binding was reduced in the presence of the free agonist VAP at 10 μM in MCF7 cells because the fluorescence of Qdots-VAP was significantly decreased when displaced by free VAP. The high binding of Qdots-VAP in the MCF7 cells was due to the higher expression of $SSTR_2$ (Abdellatif, 2015a,b).

In order to confirm the binding of Qdots-VAP to $SSRT_2$, MCF7 cells were examined using a flow cytometer (FACS). The results obtained from FACS showed higher binding of Qdots-VAP to MCF7 cells (Fig. 6). Additionally, the fluorescence intensities of Qdots-VAP to MCF7 cells reflect the same results obtained by CLSM. The studies showed that the higher binding of Qdots-VAP with these cells (MCF7 cells) were due to higher expression of mRNA of $SSTR_2$ with MCF7 cells as reported previously by

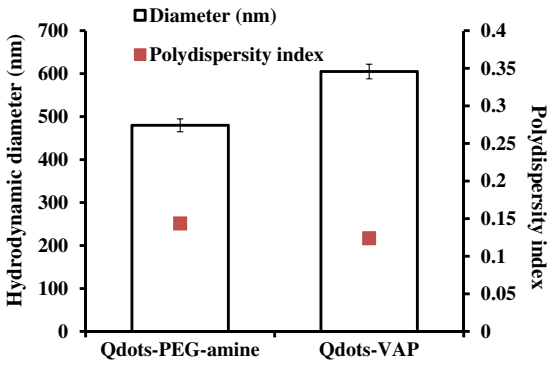

Fig. 2. Particle size distribution of Qdots-PEG-amine and Qdots-VAP which were measured using dynamic light scattering.

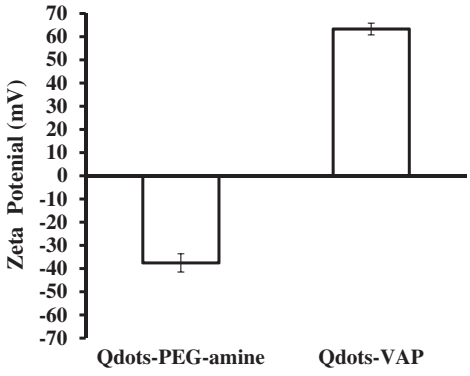

Fig. 3. Zeta potential of Qdots-PEG-amine and Qdots-VAP in phosphate buffer pH 7.4. The zeta potential of Qdots-VAP showed reversal to positive values.

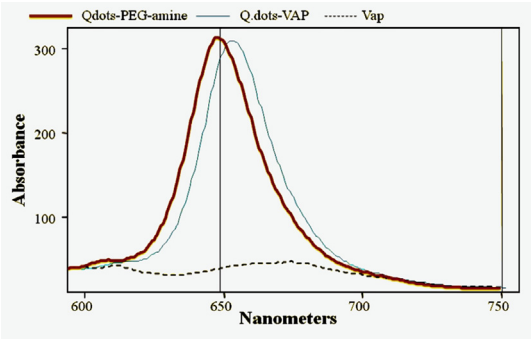

Fig. 4. Fluorescence emission spectra of VAP, Qdots-PEG-amine, Qdots-VAP in pH 7.2 buffer (Ex: 488 nm). Concentration of Qdots-PEG-amine and Qdots-VAP; 100 nM. Concentration of VAP; 1 mM.

Abdellatif (2015a,b). The fluorescence intensity increased from 3.1 to 17.2 when using Qdots-PEG-amine and Qdots-VAP respectively ($P < 0.001$) and decreased by the addition of free VAP to be12.1 MFU ($P < 0.05$).

Qdots-VAP can be fully displaced from their $SSTR_2$ when the receptors were entirely occupied with free VAP (Fig. 7) (Litau et al., 2015). The displacement was confirmed using IC_{50} for VAP and Qdots-VAP. The IC_{50} value for VAP in MCF7 cells with Qdots-VAP is approximately 700 μM. This strong binding could be an explanation for binding of Qdots-VAP with cells when Qdots carry a number of VAP on their surface can target $SSTR_2$, and the $SSTR_2$ can be occupied and blocked using VAP in a high concentration of around 700 μM. Also, the results obtained confirmed the safety of the formulated particles.

3.3. In vivo study

Recent *in vivo* studies were performed to investigate the targeting of Qdot conjugated VAP in the healthy rat (Abdellatif and Tawfeek, 2016). The bio-distribution of Qdots-VAP was assessed by determining the cadmium mass (Cd) in blood and other organs by using inductively coupled plasma mass spectrometry (ICP-MS)

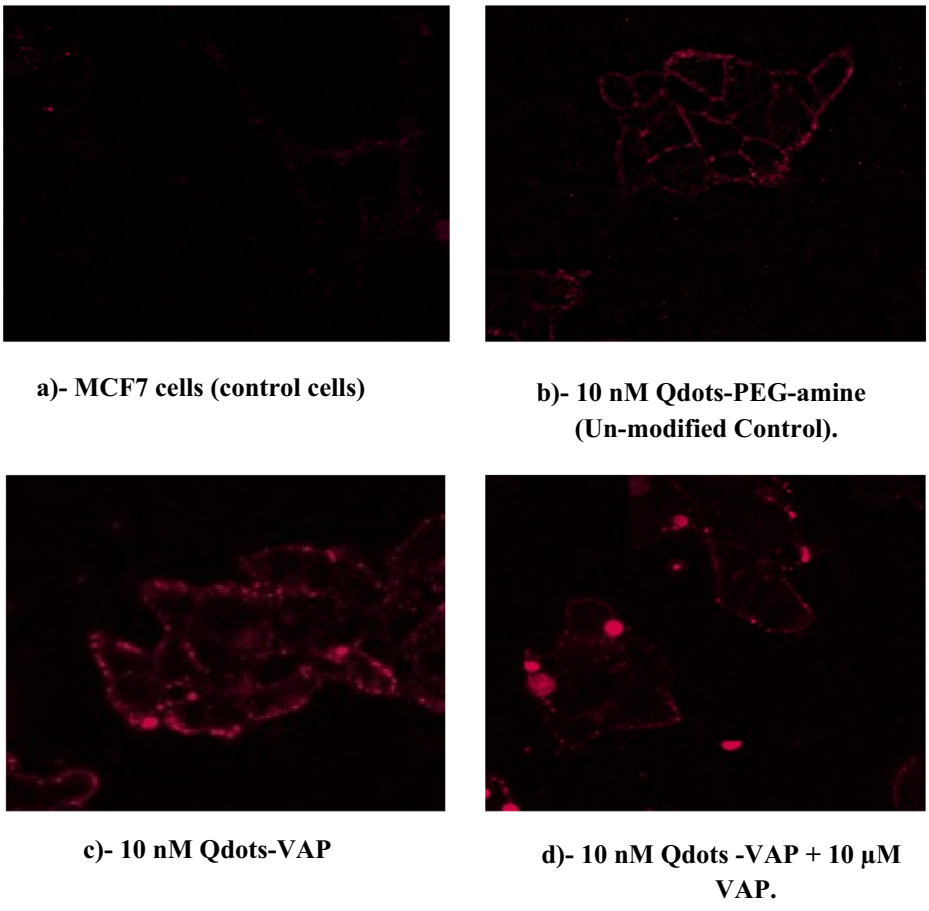

Fig. 5. Confocal microscopy images of Qdots-VAP incubated with MCF7 cells. The concentration used was 10 nM Qdots-VAP in presence or absences of 10 μM free VAP at 30 min incubation, cell medium: Leibovitźs L-15; 0.1 BSA. CLSM (EX: 488/Em: 655).

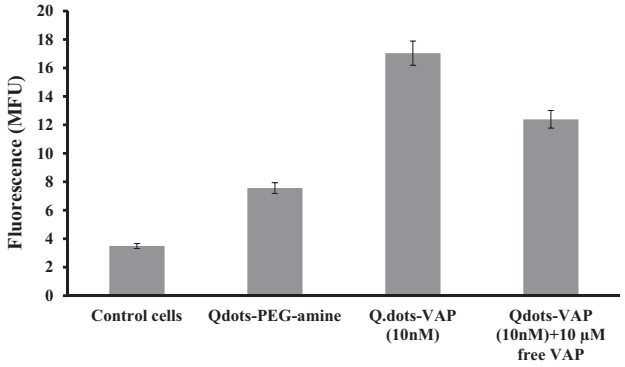

Fig. 6. Flow cytometry of Qdots-VAP with MCF7 cells. (a) Cells were incubated with 10 nM of Qdots-VAP. (b) The Qdots-VAP exhibited binding to the cell surfaces and was displaced with 10 μM of free VAP.

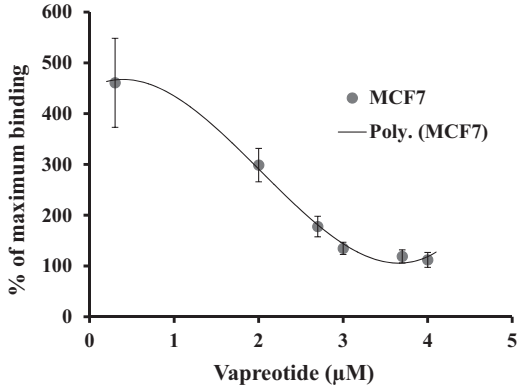

Fig. 7. Displacement curves of VAP from MCF7 cells. Concentration of 10 nM Qdots-VAP was displaced using different concentrations from 1 to 5 μM of free VAP as competitor.

which represent the concentration of Qdots-PEG-amine or Qdots-VAP in all organs of the body per one kilogram. The results showed a huge accumulation of Cd in the blood compared to the other investigated organs (Fig. 8). The percent of Cd in the blood of rat injected with Qdots-VAP was 72.09% ID/g_{tissue} of the measured fluorescence intensity. 5.9% ID/g_{tissue} were detected in the liver and 6.6% ID/g_{tissue} in the spleen. The data displayed an inhibition of the non-specific distribution of Cd in the liver compared to Qdots-PEG-amine, which was mostly accumulated in the liver.

4. Discussion

Qdots-VAP was synthesized to provide a stable colloidal solution and showed no visible coalescence. The role of EDTA in the reaction was to chelate divalent metal ions, which can oxidize sulfhydryls. Triethanolamine buffer was used in the reaction to ionize the Traut́s reagent. Our results indicate that Qdots coated with VAP has no significant different fluorescence properties compared to the unmodified Qdots-PEG-amine. Even though the Qdots-PEG-amine was chemically modified with VAP, they still possess a significant fluorescence. This indicates that the coating of Qdots with VAP did not affect the fluorescence of Qdots-PEG-amine. The polydispersity index (PDI), size (hydrodynamic diameter) and the zeta potential of particles are factors signifying the stability of NPs. PDI is a sign for the stability of NPs since it shows the size distribution range in the colloidal solution and smaller PDI values indicate the homogeneity of the particle size in the solution. A PDI below 0.7 was suitable and acceptable since the particle size distribution fell within a narrow range (Abdellatif et al., 2016). The surface charge also plays an essential role in the stability of the NPs, and the degree of zeta potential confirms the stability of the colloidal system (Abdellatif and Abou-Taleb, 2016). The high zeta potentials provide a more stable dispersion. DLS showed a reversal of zeta potential to positive values. The high zeta potential indicates the dispersion stability and the inversion of the zeta potential points out that the VAP binds to Qdots-PEG-amine (Greenwood and Kendall, 1999). Nevertheless, a significant red shift confirmed that Qdots-PEG-amine conjugated VAP. Even though the Qdots-PEG-amine was chemically modified with VAP, they still possess a significant fluorescence. This result indicates that the conjugation with VAP did not affect the fluorescence of Qdots-PEG-amine.

The results obtained from CLSM can also support our hypothesis. The results obtained with the CLSM displayed that the particles were effectively transported into the target cells. The fluorescence was recognizable and looks like spots in the cytoplasm which are typical of endocytic vesicles formed upon receptor-mediated endocytosis. Furthermore, the fluorescence intensities obtained from FACS corresponded to the results obtained by CLSM. The higher binding of Qdots-VAP to cells that expressed higher $SSTR_2$, due to higher expression of mRNA of SSTR2 with MCF7 cells as reported previously (Abdellatif, 2015a,b; Abdellatif et al., 2016). Our data showed that the Qdots-VAP exhibited a high specific binding to the $SSTR_2$ and can be displaced from their receptor by using high concentrations of the receptor agonist. These receptor-interactions and receptor-mediated endocytosis is essential to

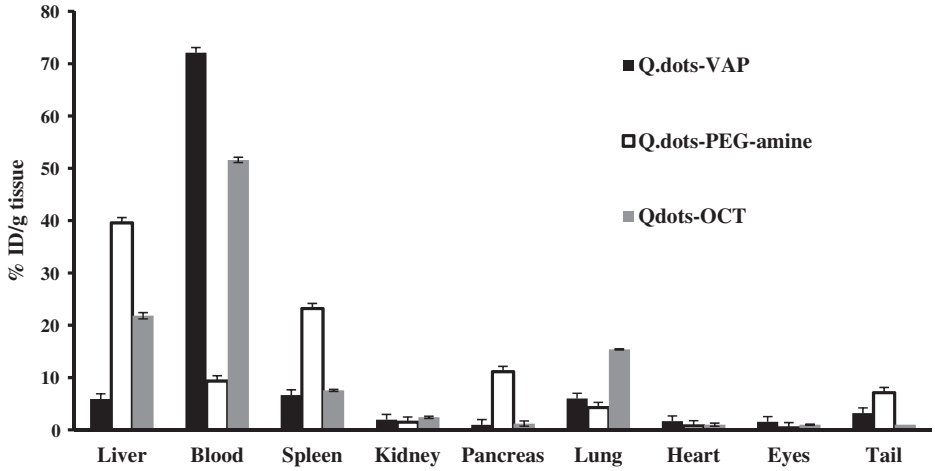

Fig. 8. Bio-distribution of Qdots-VAP and Qdots-PEG amine in various tissues of rats. The results are presented as means ± SD in %ID/g (percentage injected dose per gram tissue statistic). The results showed a massive accumulation of cadmium in the blood cells as compared to the investigated organs.

diagnose cancer cells. Qdots-VAP can be completely displaced from the receptors when the receptors were completely occupied as a good confirmation for specific receptor targeting. Finally, Qdots-VAP can act as targeting tools on $SSTR_2$.

The results obtained from *in vivo* study showed that SSTRs especially $SSTR_2$ can be targeted in the blood cells and VAP was more specific binding to $SSTR_2$ in the blood cells rather than other organs. These results will open the gate for focusing on the targeting RBCs. It was reported that the long circulation of Qdots-VAP could be due to PEGylation of Qdots-VAP. Furthermore, PEGylation is still the most widely used strategy method because a strategy cannot be used to enhance the circulation half-life of all kinds of NPs in the blood cells (Huang et al., 2016). It was stated that the PEG layer around the NPs reduced the adsorption of opsonins and other serum proteins could be reduced by the presence of PEG on the surface of NPs (Vannucci et al., 2012, Xin et al., 2012; Simsek et al., 2013). Here we found that the unmodified Qdots which carry PEG amine on its surface showed a high accumulation in the liver, which cannot explain the long circulation time of the formulated Qdots-VAP because VAP binds to the SSTR2 expressed in blood cells (Bhathena and Recant, 1980; Perez et al., 2003; Lichtenauer-Kaligis et al., 2004; Petrak, 2005; Reynaert et al., 2007; ter Veld et al., 2007; Muscarella et al., 2011). The SSTRs overexpressed on RBCs could so interact with Qdots-VAP expressed in RBCs. High accumulation of Cd in the blood cells in case of injected Qdots-VAP due to the expression of SSTRs on the blood cells and VAP binds to $SSTR_2$ expressed in blood cells (Zahr et al., 2006). VAP which coated the Qdots to target blood cells that over-expressed SST2 receptors in their surfaces will be investigated in our research group for delivery of the same Qdots coated with SST for future targeting of blood cells (Abdellatif et al., 2018). Qdots coated with VAP has higher specific targeting and more specific internalization compared with Qdots coated with SST. This type of NPs which one VAP or SST or both will open the gate for new kind of targeting blood cells disease such as Leukaemia. It has been reported that SSTRs were identified on mitogen-activated human peripheral blood lymphocytes (PBL) and human leukemic cells in 87.5% of lymphoblastic leukaemia and in 12.5% of non-lymphocytic leukaemia, using a somatostatin radio-binding assay (Hiruma et al., 1990). Thus, the targeting of leukemic cells using Qdots coated with somatostatin analogues such as VAP or OCT, open up a new venue for new possibilities of detecting and treatment of leukemic cells.

5. Conclusions

Somatostatin receptor 2 showed high specific interaction with the synthesized Qdots coated with somatostatin analogues. The specific binding of Qdots-VAP was also maintained by displacement experiments to confirm the specific binding to $SSTR_2$. The *in vivo* experiments showed the bio-distribution of Qdots-VAP traveled to each organ with massive accumulation in blood cells which are useful tools for cancer imaging and treatment. The targeting of blood cells using Qdots coated with somatostatin analogues VAP open the gate for new possibilities of detecting and treatment of many kinds of blood diseases. Furthermore, the targeted Qdots has a fluorescence as proved by a fluorimeter, FACS, and CLSM, so this kind of nanoparticles can be also used in bio-imaging for cancer cells.

References

Abdellatif, A., 2015a. Octreotide labelled fluorescein isothiocyanate for identification of somatostatin receptor subtype 2. Biochem. Physiol. 4 (183), 2.

Abdellatif, A.A., 2015b. Targeting of somatostatin receptors using quantum dots nanoparticles decorated with octreotide. J. Nanomed. Nanotechnol. S6, 1.

Abdellatif, A.A., Abou-Taleb, H.A., 2016. Transfersomal nanoparticles of keratolytic and antibacterial agents for enhanced transdermal delivery. J. Nanotechnol. Adv. Mater. 4, 19–23.

Abdellatif, A.A., Tawfeek, H.M., 2016. Transfersomal nanoparticles for enhanced transdermal delivery of clindamycin. AAPS PharmSciTech 17 (5), 1067–1074.

Abdellatif, A.A. et al., 2016. Novel gold nanoparticles coated with somatostatin as a potential delivery system for targeting somatostatin receptors. Drug Dev. Ind. Pharm., 1–10

Abdellatif, A.A.H. et al., 2018. Somatostatin decorated quantum dots nanoparticles for targeting of somatostatin receptors. Iranian J. Pharm. Res. 17 (2), 513–524.

Akita, S. et al., 2016. Early detection of lymphatic disorder and treatment for lymphedema following breast cancer. Plast Reconstr. Surg. 138 (2), 192e–202e.

Amartey, J.K., 1993. Technetium-99m labeled somatostatin and analogs: synthesis, characterization and in vivo evaluation. Nucl. Med. Biol. 20 (4), 539–543.

Avvakumova, S. et al., 2016. Theranostic nanocages for imaging and photothermal therapy of prostate cancer cells by active targeting of neuropeptide-Y receptor. Bioconjug. Chem. 27 (12), 2911–2922.

Ballou, B. et al., 2005. Fluorescence imaging of tumors in vivo. Curr. Med. Chem. 12 (7), 795–805.

Bertrand, N., Leroux, J.C., 2012. The journey of a drug-carrier in the body: An anatomo-physiological perspective. J. Control. Release 161 (2), 152–163.

Bhathena, S.J., Recant, L., 1980. Somatostatin receptors on circulating human blood cells. Horm. Metab. Res. 12 (6), 277–278.

Chen, H.P. et al., 2009. Inhibition of photobleaching and blue shift in quantum dots. Chem. Commun. 13, 1676–1678.

Cheng, M. et al., 2013. Synthesis of liver-targeting dual-ligand modified GCGA/5-FU nanoparticles and their characteristics in vitro and in vivo. Int. J. Nanomed. 8, 4265–4276.

Davidson, R.A. et al., 2015. Evolution of silver nanoparticles in the rat lung investigated by X-ray absorption spectroscopy. J. Phys. Chem. A 119 (2), 281–289.

Derwin, K.A. et al., 2012. Low-dose CT imaging of radio-opaque markers for assessing human rotator cuff repair: accuracy, repeatability and the effect of arm position. J. Biomech. 45 (3), 614–618.

Destremaut, F. et al., 2009. Microfluidics with on-line dynamic light scattering for size measurements. Lab Chip 9 (22), 3289–3296.

Fang, M. et al., 2013. In vitro invasive pattern of hepatocellular carcinoma cell line HCCLM9 based on three-dimensional cell culture and quantum dots molecular imaging. J. Huazhong Univ. Sci. Technolo. Med. Sci. 33 (4), 520–524.

Ghasemi, Y. et al., 2009. Quantum dot: magic nanoparticle for imaging, detection and targeting. Acta Biomed. 80 (2), 156–165.

Greenwood, R., Kendall, K., 1999. Selection of suitable dispersants for aqueous suspensions of zirconia and titania powders using acoustophoresis. J. Eur. Ceram. Soc. 19 (4), 479–488.

Gupta, K. et al., 1999. Binding and displacement of vascular endothelial growth factor (VEGF) by thrombospondin: effect on human microvascular endothelial cell proliferation and angiogenesis. Angiogenesis 3 (2), 147–158.

Gupta, P. et al., 2017. Assessment of near-infrared fluorophores to study the biodistribution and tumor targeting of an IL13 receptor alpha2 antibody by fluorescence molecular tomography. Oncotarget 8 (34), 57231–57245.

Herrmann, K. et al., 2015. Biodistribution and radiation dosimetry for the chemokine receptor CXCR4-targeting probe 68Ga-pentixafor. J. Nucl. Med. 56 (3), 410–416.

Hiruma, K. et al., 1990. Somatostatin receptors on human lymphocytes and leukaemia cells. Immunology 71 (4), 480–485.

Hoyer, D. et al., 1995. Classification and nomenclature of somatostatin receptors. Trends Pharmacol. Sci. 16 (3), 86–88.

Huang, H. et al., 2016. Axial PEGylation of tin octabutoxy naphthalocyanine extends blood circulation for photoacoustic vascular imaging. Bioconjug. Chem. 27 (7), 1574–1578.

Kane, P.F., Hall Jr., W.L., 2006. Determination of arsenic, cadmium, cobalt, chromium, lead, molybdenum, nickel, and selenium in fertilizers by microwave digestion and inductively coupled plasma-optical emission spectrometry detection: collaborative study. J. AOAC Int. 89 (6), 1447–1466.

Kwon, K.C. et al., 2016. Enhanced in vivo tumor detection by active tumor cell targeting using multiple tumor receptor-binding peptides presented on genetically engineered human ferritin nanoparticles. Small 12 (31), 4241–4253.

Leung, A.B. et al., 2006. Particle-size and velocity measurements in flowing conditions using dynamic light scattering. Appl. Opt. 45 (10), 2186–2190.

Li, D. et al., 2013. Cancer therapy and fluorescence imaging using the active release of doxorubicin from MSPs/Ni-LDH folate targeting nanoparticles. Biomaterials 34 (32), 7913–7922.

Lichtenauer-Kaligis, E.G. et al., 2004. Differential expression of somatostatin receptor subtypes in human peripheral blood mononuclear cell subsets. Eur. J. Endocrinol. 150 (4), 565–577.

Litau, S. et al., 2015. Next generation of SiFAlin-based TATE derivatives for PET imaging of SSTR-positive tumors: influence of molecular design on in vitro SSTR binding and in vivo pharmacokinetics. Bioconjug. Chem. 26 (12), 2350–2359.

Muscarella, L.A. et al., 2011. Gene expression of somatostatin receptor subtypes SSTR2a, SSTR3 and SSTR5 in peripheral blood of neuroendocrine lung cancer affected patients. Cell. Oncol. (Dordr.) 34 (5), 435–441.

Othman, M. et al., 2017. Preparation and evaluation of 5-fluorouracil loaded microsponges for treatment of colon cancer. J. Cancer Sci. Ther. 9, 307–313.

Patel, Y.C., 1999. Somatostatin and its receptor family. Front Neuroendocrinol. 20 (3), 157–198.

Perez, J. et al., 2003. Somatostatin binds to murine macrophages through two distinct subsets of receptors. J. Neuroimmunol. 138 (1–2), 38–44.

Petrak, K., 2005. Essential properties of drug-targeting delivery systems. Drug Discov. Today 10 (23–24), 1667–1673.

Phatak, P. et al., 2007. Telomere uncapping by the G-quadruplex ligand RHPS4 inhibits clonogenic tumour cell growth in vitro and in vivo consistent with a cancer stem cell targeting mechanism. Br. J. Cancer 96 (8), 1223–1233.
Pilz, K. et al., 2016. Vertebral fractures - An underestimated side-effect in patients treated with radio(chemo)therapy. Radiother. Oncol. 118 (3), 421–423.
Potier, A. et al., 2016. Early detection of cancer therapeutics-related cardiac dysfunction. Bull. Cancer.
Prescott, M. et al., 2003. The 2.2 A crystal structure of a pocilloporin pigment reveals a nonplanar chromophore conformation. Structure 11 (3), 275–284.
Reynaert, H. et al., 2007. Expression of somatostatin receptors in splanchnic blood vessels of normal and cirrhotic rats. Liver Int. 27 (6), 825–831.
Schneider, G. et al., 2016. Induction of a tumor-metastasis-receptive microenvironment as an unwanted side effect after radio/chemotherapy and in vitro and in vivo assays to study this phenomenon. Methods Mol. Biol.
Simsek, S. et al., 2013. Brain targeting of atorvastatin loaded amphiphilic PLGA-b-PEG nanoparticles. J. Microencapsul. 30 (1), 10–20.
Sreenivasan, V.K.A. et al., 2012. Targeting somatostatin receptors using in situ-bioconjugated fluorescent nanoparticles. Nanomedicine 7 (10), 1551–1560.
ter Veld, F. et al., 2007. Somatostatin receptor expression in peripheral blood of type 2 diabetes mellitus patients. Horm. Metab. Res. 39 (3), 230–232.
Tsoi, K.M. et al., 2013. Are quantum dots toxic? Exploring the discrepancy between cell culture and animal studies. Acc. Chem. Res. 46 (3), 662–671.
Updegrove, T.B. et al., 2011. The stoichiometry of the Escherichia coli Hfq protein bound to RNA. Rna-a Publication of the Rna Society 17 (3), 489–500.
Vannucci, L. et al., 2012. Selective targeting of melanoma by PEG-masked protein-based multifunctional nanoparticles. Int. J. Nanomed. 7, 1489–1509.
Wang, Y.F. et al., 2008. Determination of lead, cadmium, mercury, chromium and arsenic in acrylonitrile-butadiene-styrene copolymer using microwave digestion-ICP-MS. Guang Pu Xue Yu Guang Pu Fen Xi 28 (1), 191–194.
Xin, H. et al., 2012. Anti-glioblastoma efficacy and safety of paclitaxel-loading Angiopep-conjugated dual targeting PEG-PCL nanoparticles. Biomaterials 33 (32), 8167–8176.
Zahr, A.S. et al., 2006. Macrophage uptake of core-shell nanoparticles surface modified with poly(ethylene glycol). Langmuir 22 (19), 8178–8185.